# CHAPTER 4 RESULTS AND DISCUSSION

The experimental results in previous chapter will be discussed here. The discussion outlines the processes of this research work from varying thickness of DLC/a-Si thin film stack ratio using PFCA technique on germanium wafer substrate. Then, DLC/a-Si thin films stack growth rate with various wafer substrates, including germanium, tantalum and silicon, respectively was evaluated and finally thin film stack layer thickness & composition, morphology, bonding structure of DLC/a-Si were discussed.

## 4.1 Results on Varying Thickness of DLC/a-Si Thin Film Stack Ratio

### 4.1.1 Thickness and Morphology of Film Stack Layer

Cross-sectional Bright-Field TEM (BF-TEM) were carried out on various bi-layer films deposited by RF-magnetron sputtering for a-Si and pulse-filtered cathodic arc for DLC. The thickness stack configuration is described in the experimental section. Deposited thickness of both a-Si and DLC films were controlled via in-situ ellipsometer. Based on the TEM contrast and morphology, the deposited film stacks are amorphous in nature for all deposited film stack configurations as shown in Figure 4.1.

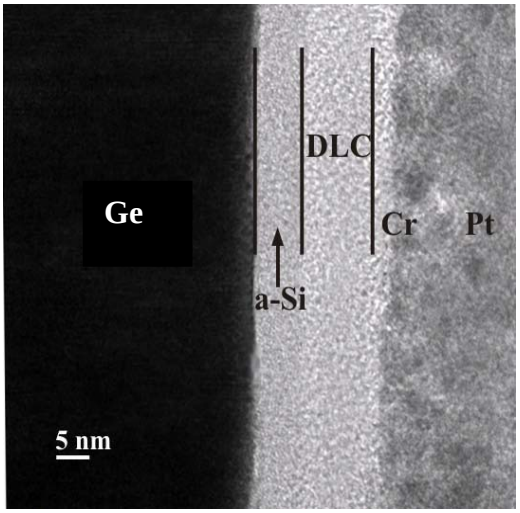


**Figure 4.1** Magnified TEM image of bi-layer DLC/a-Si film.

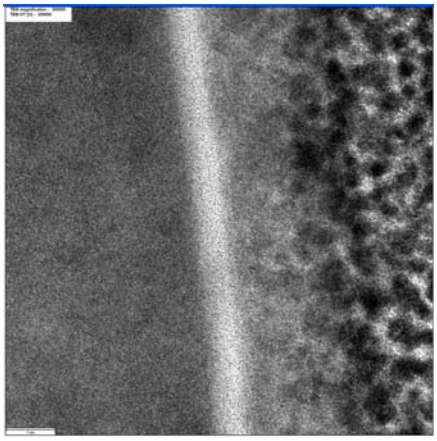

(a) DLC/a-Si 2/2 nm scale bar 7 nm Mag 300,000

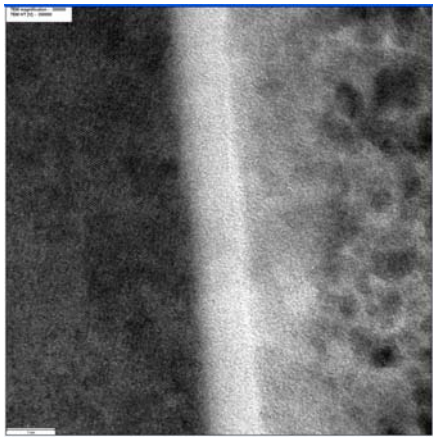

(b) DLC/a-Si 6/2 nm scale bar 7 nm Mag 300,000

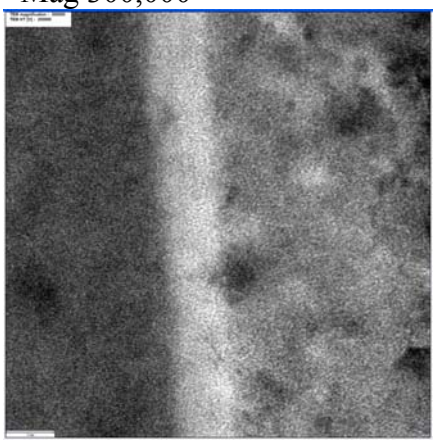

(c) DLC/a-Si 4/4 nm scale bar 7 nm Mag 300,000

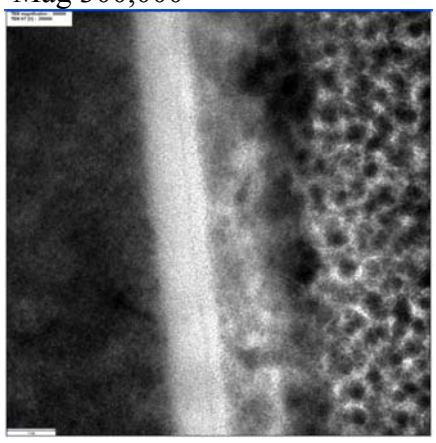

(d) DLC/a-Si 2/6 nm scale bar 7 nm Mag 300,000

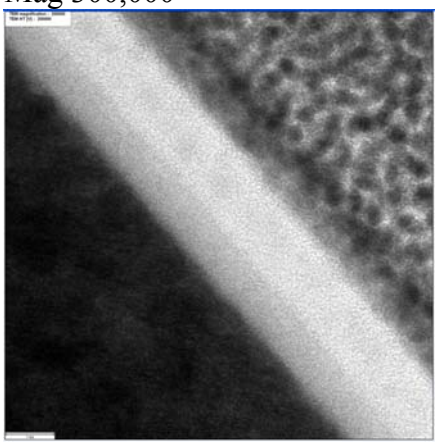

(e) DLC/a-Si 6/6 nm scale bar 7 nm Mag 300,000

**Figure 4.2** TEM images of bi-layer DLC/a-Si for all films stack.

Total film stack thickness was measured from TEM images in Figure 4.2 (a–e) and the results are shown in Table 4.1.

**Table 4.1** In-situ ellipsometer monitored thickness value and TEM total thickness

| Item | DLC/a-Si | TEM total thickness |
|---|---|---|
| 1 | 2/2 | 3.82 |
| 2 | 2/6 | 8.41 |
| 3 | 4/4 | 8.74 |
| 4 | 6/2 | 8.23 |
| 5 | 9/6 | 15.66 |

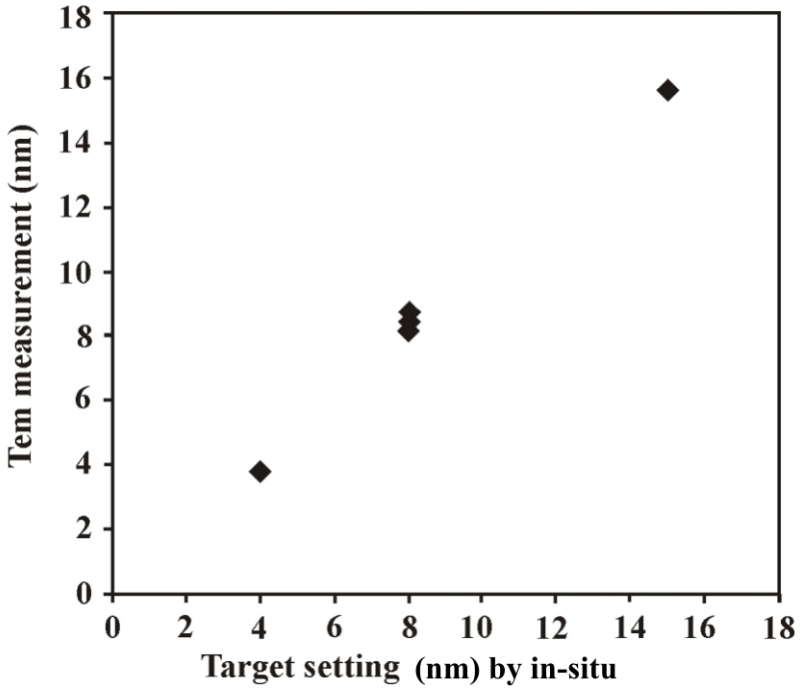


**Figure 4.3** Comparison of the thickness as monitored by in-situ ellipsometer and TEM.

A good correlation between TEM-measured total film stack thickness versus the sum of the individual in-situ ellipsometer-measured a-Si and DLC thicknesses was found as shown in Figure 4.3. However, from the BF-TEM we were not able to delineate the a-Si and DLC layer within the stack for all Si and C stack combinations because there was not sufficient contrast in the BF-TEM. TEM showed that when the a-Si thickness is lower than 6 nm, there was not sufficient difference of contrast between the a-Si and DLC layers. Only when the as-deposited a-Si thickness is higher than 6 nm in the total bilayer stack), BF-TEM start showing a layer with darker contrast located at right next to the substrate. Figure 4.4(a) and (b) shows location and the measured thickness of this darker layer which strongly suggested that this corresponds to the a-Si layer.

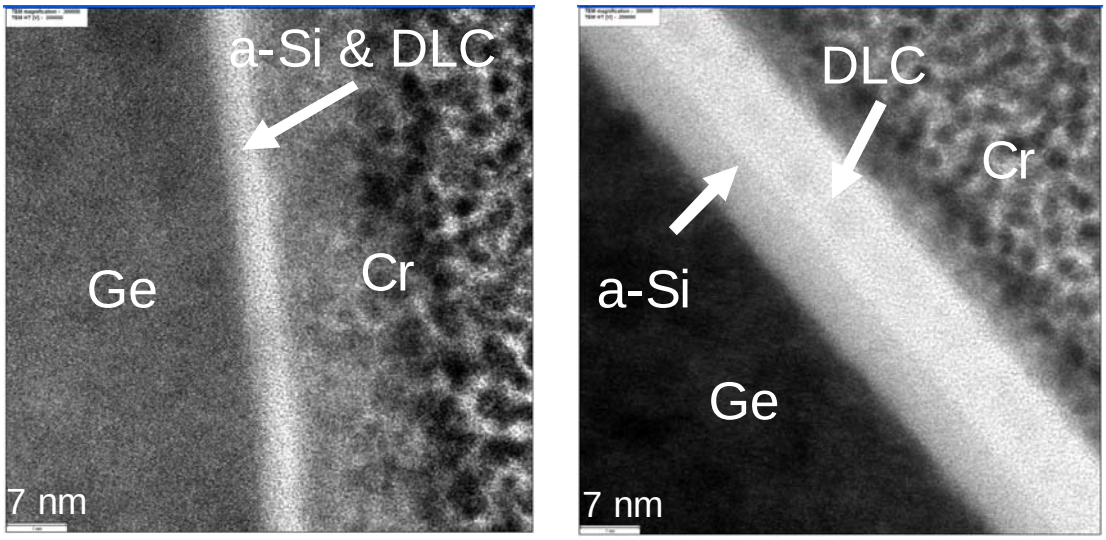


(a) (b)

**Figure 4.4** (a) DLC/a-Si 2/2 nm scale bar 7 nm, magnification 300,000
(b) DLC/a-Si 9/6 nm scale bar 7 nm, magnification 300,000

Surface roughness morphology was performed using AFM and results are shown in Figure 4.5(b–f). Table 4.2, shows measured surface roughness (Ra) from DLC/a-Si film stack coated at various a-Si and DLC thickness ratios. The amount of smoothening effect of the coated a-Si/DLC film is independent of the coating thickness.

**Table 4.2** Summary of bi-layer DLC/a-Si thin film stack ratio and surface roughness (Ra)

| DLC (nm) | a-Si (nm) | DLC/a-Si thickness ratio | Total thickness (nm) | Roughness (Ra) (nm) |
|---|---|---|---|---|
| - | - | Ge substrate | - | 0.72 |
| 2 | 2 | 2/2 | 4 | 0.25 |
| 2 | 6 | 2/6 | 8 | 0.26 |
| 4 | 4 | 4/4 | 8 | 0.27 |
| 6 | 2 | 6/2 | 8 | 0.21 |
| 9 | 6 | 9/6 | 15 | 0.25 |

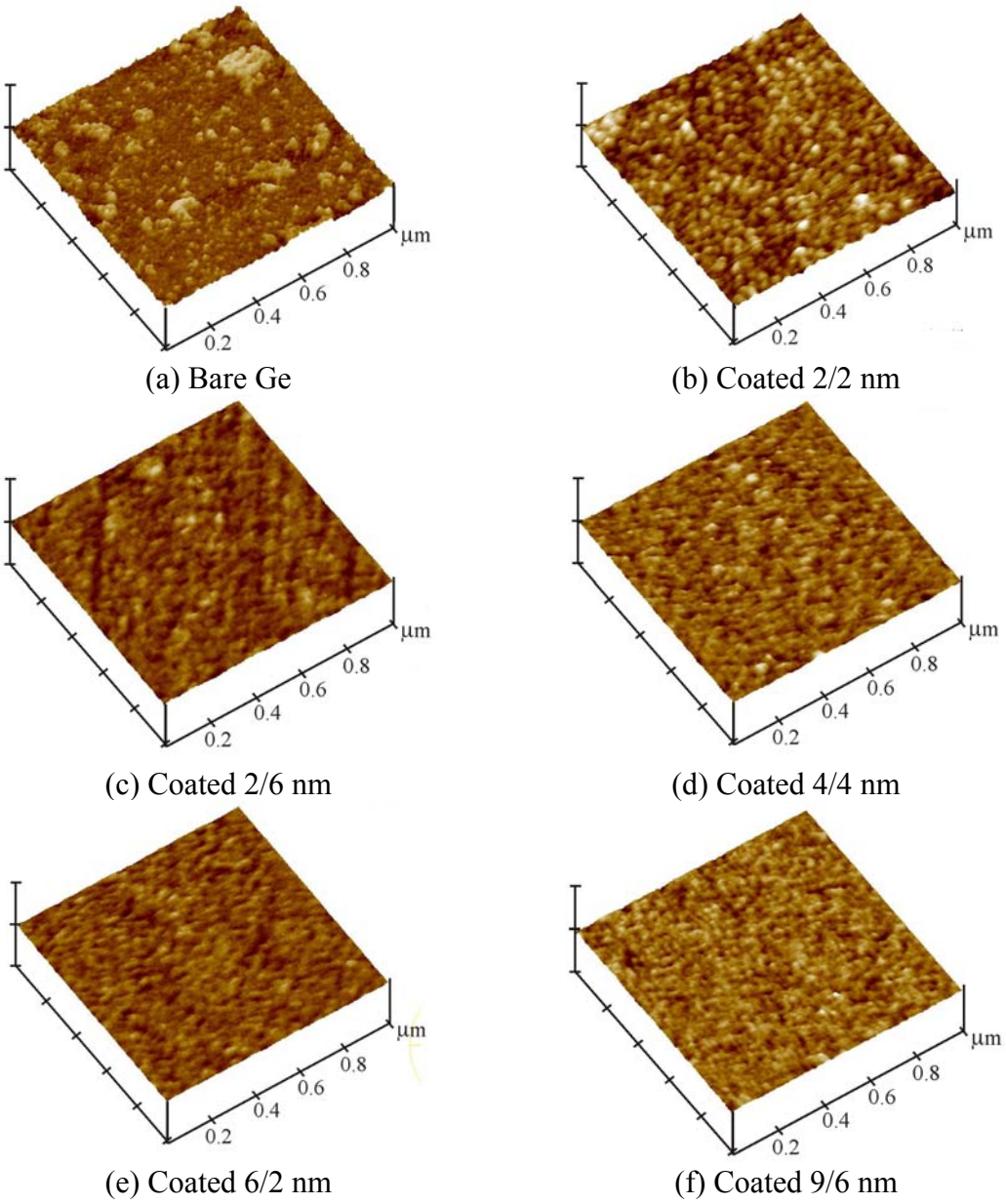


(a) Bare Ge (b) Coated 2/2 nm

(c) Coated 2/6 nm (d) Coated 4/4 nm

(e) Coated 6/2 nm (f) Coated 9/6 nm

**Figure 4.5** (a-f) Surface roughness of DLC/a-Si films deposited at different DLC/a-Si ratios on Ge substrate**.**

### 4.1.2 Film Stack Validation Via Spectroscopic Ellipsometry

Spectroscopic Ellipsometry (SE) was used as a non-destructive characterization method to further validate film stack information. Both cross-section TEM and depth-sputtered XPS are destructive thin characterization methods. On the other hand, SE used in this study is non-destructive because it employs white light reflected off the film to measure the change in polarization expressed as Ψ and Δ. The non-destructive nature of SE was utilized in this study to delineate any sample preparation artifacts and potentially to capture any subtle features within the film stack.

### 4.1.2.1 Structure of Sample Evaluation

First interface layer between DLC and a-Si need to be evaluated. The high magnification 1,000,000x of cross-sectional TEM image of DLC/a-Si film in Figure 4.6(a) shows that there are three regions of our interest, including a-Si, SiC and DLC. The morphology and density of the film in each region are obviously different as shown in white and gray and are also clearly seen in Figure 4.6(b) which is the cropped image of Figure 4.6(a) after brightness and contrast adjustment.

In the a-Si region, the morphology of the cross-sectional film is a random structure. The film thickness is slightly less than that of the setting value, 6 nm. Decrease in thickness may be resulted from the depth of maximum carbon implantation into a-Si layer and the formation of a new phase of SiC. Density of a-Si clusters in this region becomes denser toward Ge surface. The difference in the film density may possibly be explained either by the heterogeneous nucleation behavior of the film itself (i.e. plenty of a-Si structures can be nucleated and formed immediately on Ge surface since it reduces the energy barrier to nucleation of a-Si [84]) or by the diffusion of Si atoms due to the SiC nucleation [85]. However, to have better understanding on these phenomena, further experiments may be required.

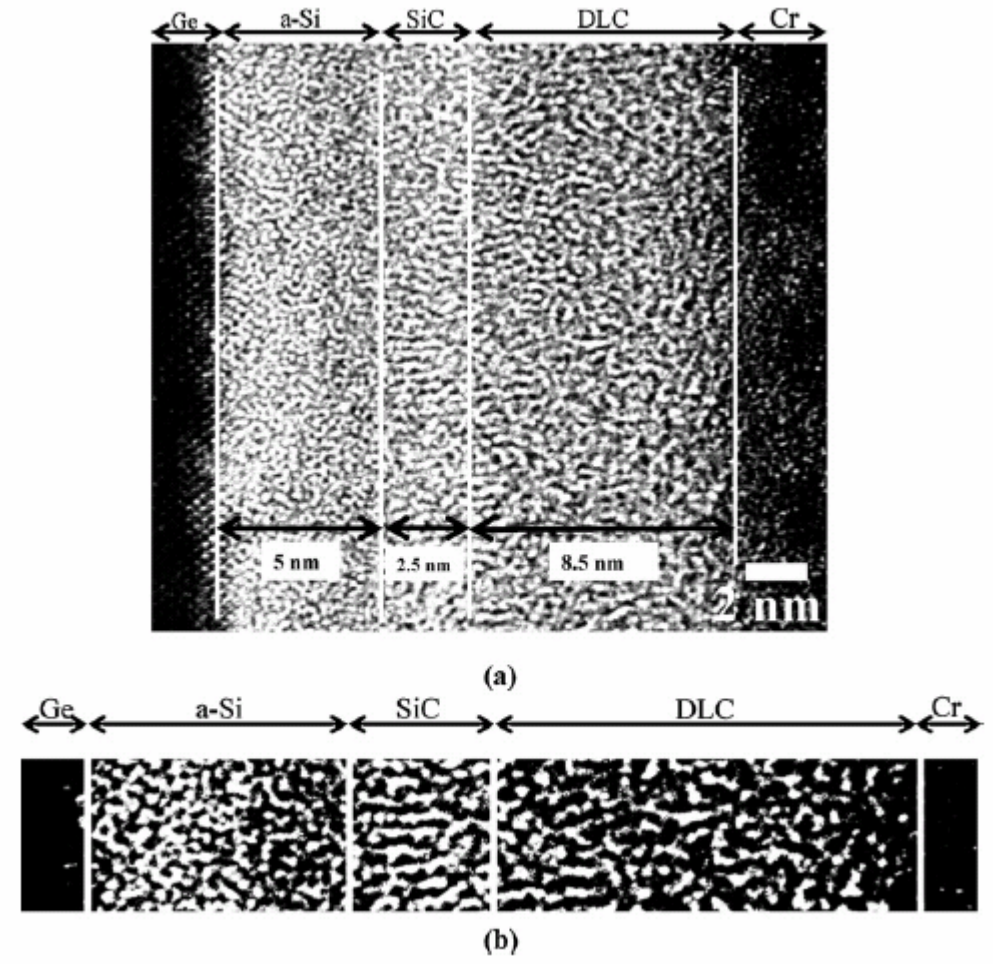


**Figure 4.6** Cross-sectional TEM image (×1,000,000) of the films (a) and cropped image from (a) with a brightness and contrast adjustment to provide a clear vision on the cross-sectional morphology of the films (b).

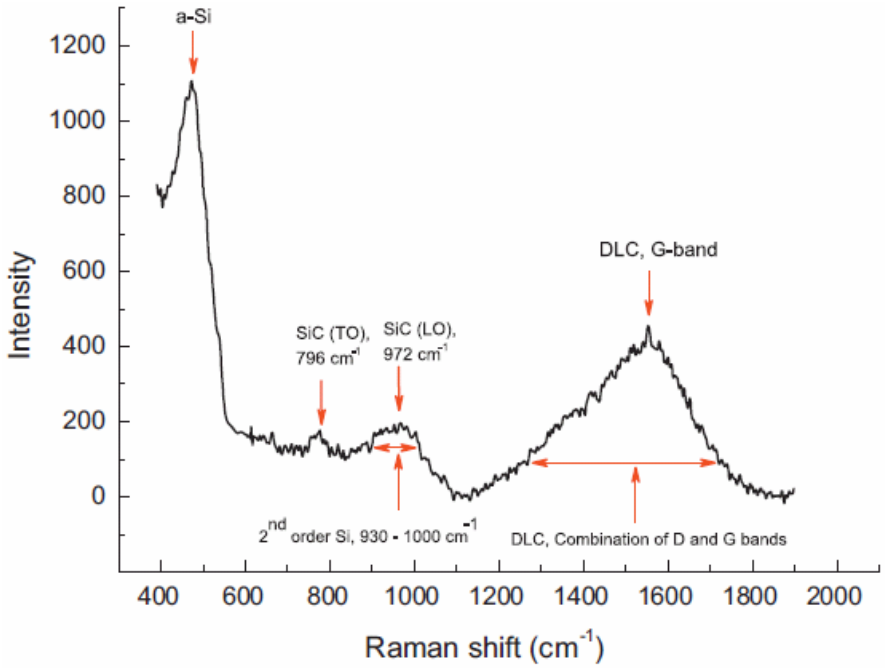


**Figure 4.7** Raman spectra of DLC/a-Si film with a thickness of 9/6 nm.

Many incoming carbon ions from the source continuously deposit on a-Si layer to form the DLC film. However, the carbons impinging on a-Si layer may act not only as the carbon source for DLC film formation, but also as a source for the SiC formation. At the SiC region, the column-like structure of SiC can be observed as shown in Figure 4.6(b), which is in agreement with that observed by Lindner [85]. When carbon atoms transported to a-Si layer, they have enough kinetic energy to penetrate the a-Si layer and chemically react with Si atoms to form SiC to gain a thermodynamic stability. Thickness of this SiC layer is approximately 2.5 nm, which was estimated from the difference in the layer morphology. It should be noted that many factors such as surface roughness of a-Si layer and depth of carbon penetration may result in non-uniform film thickening.

When the flows of carbon atoms are still continued, many of them are not in equilibrium with each other and, hence, react with the neighboring atoms to form DLC structure as shown in the DLC region. The film thickness is approximately 8.5 nm, which is slightly less than that of the setting value, 9 nm, since some of carbon atoms at the a-Si/DLC interface were contributed to the formation of SiC layer. The film morphology was also similar to that of the a-Si layer which is a random structure.

Raman spectroscopy was used to investigate the vibrational modes of carbon and silicon atoms due to chemical bonding, especially in SiC, at the DLC/a-Si interface. The longitudinal optical (LO) and the transversal optical (TO) phonon modes of SiC formation were observed at 796 $cm^{-1}$ and 972 $cm^{-1}$, respectively, as shown in Figure 4.7 The Raman peaks located at these positions are in agreement with those reported for 3C SiC (β-SiC) [87]. The prominent peak at 480 $cm^{-1}$ is corresponded to the vibrational mode of amorphous Si (a-Si) since it was used as a seed layer for depositing the DLC film [88]. However, no peak from crystalline silicon at 520 $cm^{-1}$ is likely to be observed. This suggests that during the deposition of a-Si layer on germanium substrate there was probably no crystalline silicon formation.

In the higher wavenumber, the broad feature in the 1100–1800 $cm^{-1}$ region is related to the vibrational modes of DLC graphitic characteristics, generally consisting of G and D bands. The maximum peak is corresponded to the G-band locating at about 1554 $cm^{-1}$, which is different from that of polycrystalline graphite locating at about 1580 $cm^{-1}$. In general the intensity ratio of G band to D band ($I_D/I_G$) is correlated to the $sp^3/sp^2$ bonding ratio, representing the physical characteristics of DLC film [89]. Ideally, the value should be close to zero. Thus, by fitting the Raman spectra, the $I_D/I_G$ ratio of DLC film is 0.45. This result confirms that much more content of the $sp^3$ of the tetrahedral amorphous carbon (ta-C) structure is presented and it is in agreement with Ferari, et al. [90].

**Table 4.3** XPS binding energy of different bonds

| Bond | Binding energy (eV) |
|---|---|
| C-C | 284-284.5 |
| C-Si (C1s) | 282.3-283.7 |
| Si-C(Si2p) | 99.8-101.3 |
| Si-Si | 99.2-99.6 |

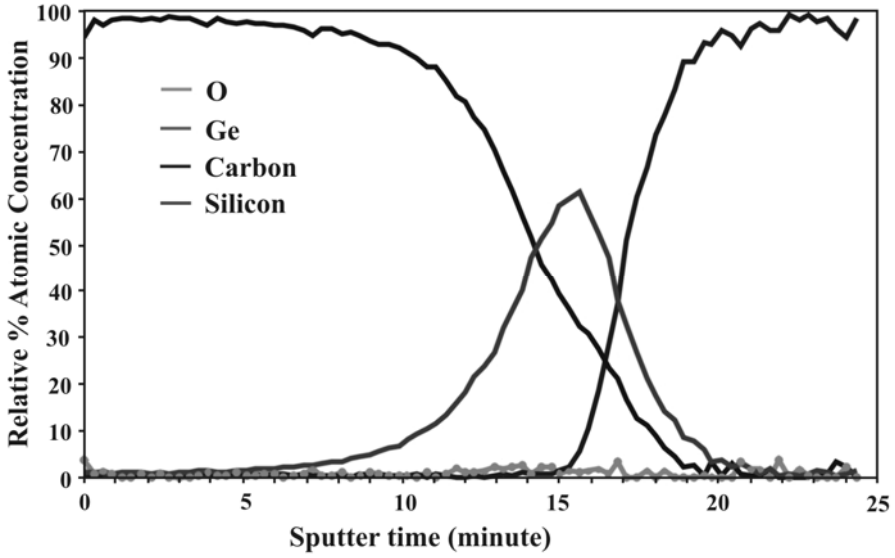


**Figure 4.8** The gross XPS chemical depth profile of DLC/a-Si film with a thickness of 9/6 nm on Ge substrate.

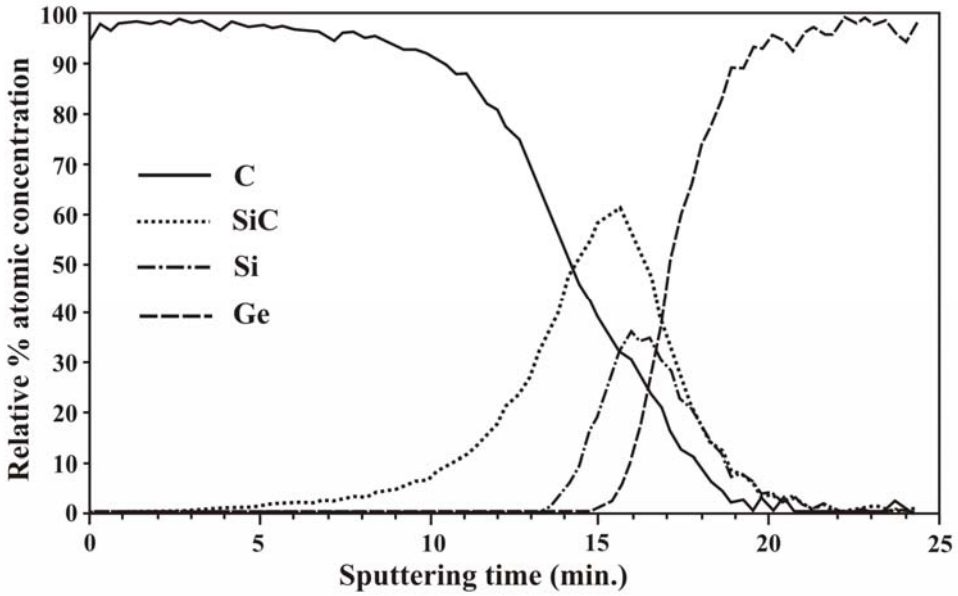


**Figure 4.9** The details XPS depth profile of DLC/a-Si film with a thickness of 9/6 nm on Ge substrate.

To have further qualitative information on SiC formation at the interface, XPS analysis was employed. Table 4.3 shows binding energies of the chemical bonds found in the DLC/a-Si film (the spectra are not shown). The highest-energy range of 284–284.5 eV is assigned to the bonding of carbon atoms (C-C) in DLC. The C-Si (C 1s) and Si-C (Si 2p) configurations, corresponding to bonding between carbon and silicon atoms in SiC, are in the ranges of 282.3–283.7 eV and 99.8–101.3 eV, respectively. The lowest energy in the range of 99.2–99.6 eV is stood for the bonding of silicon atoms (Si- Si) in the a-Si layer.

In addition, the XPS sputter depth profile was also carried out to confirm the SiC formation at the DLC/a-Si interface. The DLC/a-Si film with the setting thickness ratio of 9/6 nm was etched using ion bombardment for acquiring the information. The actual depth for each XPS analysis depends upon the etching rate (sputtering time) and the material being etched at any depth. Figure 4.8 shows a gross XPS chemical depth profile based on integrated intensity of C 1s and Si 2p core level signals–corresponding to DLC and a-Si, respectively. Figure 4.9 represents details five spectra of the depth profile ranging from DLC film (top layer), SiC layer (C-Si and Si-C), a-Si layer and germanium substrate. At the sputtering time of less than 5 min, the depth profile represents the relative atomic concentration of DLC (C-C) of more than 90%. It gradually decreases for longer sputtering time and becomes 0% at 15 min. The spectra with Gaussian distribution contributed to the SiC (C-Si and Si-C) are initially occurred at about 5 min of sputtering time and becomes maximum at 14 min with the relative atomic concentration of approximately 40%. The presence of these spectra strongly confirmed the SiC formation at the DLC/a-Si interface. The spectrum corresponding to Si-Si bonding of a-Si layer appears at 13 min of sputtering time and reaches the maximum content of 37% at 16 min. The spectrum of Ge substrate begins at 15 min and reaches the maximum value at 18 min. The overlap of the spectra implies the penetration of the atoms during film deposition.

### 4.1.2.2 Analysis Model

In this study several fitting models comprising of various DLC and Si combinations were constructed. The first model was constructed based on the nominal structure of the sample measured. The second and third models were constructed based on SiC forming in interface layer DLC/a-Si of the samples measured as shown in Figure 4.10 Film stack information of then extracted from ellipsometric data via a model dependent analysis.

As the DLC surface roughness was only 0.25 nm so that it was not necessary to take this roughness into account for our ellipsometric studies. The interface layer between DLC and a-Si can be modeled as a mixture of DLC and a-Si properties, using the Bruggeman effective medium approximation (BEMA). The DLC volume fraction for the mixture was fixed at 50% (which was an approximation DLC and a-Si defuse each other on par). Best fit between the measured and calculated $\Psi$ and $\Delta$ values was achieved via Marquardt-Levenberg algorithm [91].

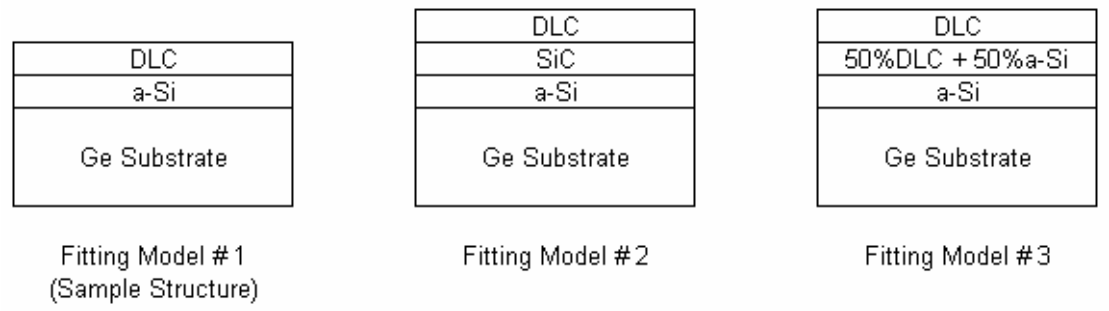


**Figure 4.10** DLC sample structure and fitting models.

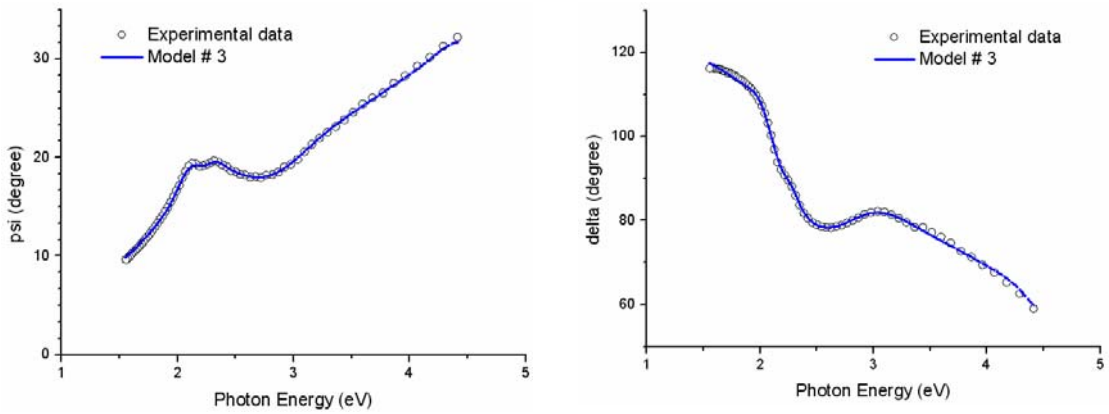


(a) Model#3 sample DLC/a-Si 9/6 nm (b) Model#3 sample DLC/a-Si 9/6 nm

**Figure 4.11** Illustration of generated and experimental data of model # 3 for the sample DLC/a-Si film stack 9/6 nm : (a) fitting on psi, (b) fitting on delta at incident angle 75.5°.

The general film stack configuration as extracted via SE analysis is in agreement with TEM and XPS. Figure 4.11(a) and (b) shows a typical measured and calculated spectra for the thicker layer sample (with DLC/a-Si 9/6 nm as controlled by in-situ ellipsometer) ), in which the optical properties of DLC and a-Si were modeled using the Tauc-Lorentz (TL) dispersion model described in the previous section. It is seen that model # 3 gives very good fits for the Ψ and Δ value for entire wavelength region, especially in the short wavelength are more sensitive to the surface structure due to the short penetration depth of light in the sample. SE also indicates that there exist a thin Si-C transition layer due to the BEMA was significant improved fitting via reduced MSE, while crystalline silicon carbide layer in model #2 unimproved, might be due to this material optical properties (From Palik I: pp. 592-593) [92] used was mismatch the existing amorphous silicon carbide interfacial layer. The thickness of each layer structure of all the bi-layer DLC/a-Si film stack and MSE from the model 3 calculations are shown in Table 4.4. The relationship between the SE total film stack thickness versus the sum of a-Si and DLC thickness as detected by in-situ ellipsometer during deposition is shown in Table 4.5 and Figure 4.12.

**Table 4.4** The thickness of each layer of all the bi-layer DLC/a-Si film stacks and MSE from SE model # 3 calculation

| Item | DLC/a-Si(nm) | DLC | EMA DLC/a-Si | a-Si | MSE | Total Thickness |
|---|---|---|---|---|---|---|
| 1 | 2/2 | 2.08±0.186 | 0±0.275 | 1.80±0.113 | 11.79 | 3.88 |
| 2 | 2/6 | 0.99±0.077 | 2.92±0.121 | 4.75±0.086 | 10.54 | 8.66 |
| 3 | 4/4 | 3.41±0.087 | 1.67±0.133 | 3.55±0.075 | 8.61 | 8.63 |
| 4 | 6/2 | 6.86±0.222 | 0±0.328 | 1.43±0.135 | 12.39 | 8.29 |
| 5 | 9/6 | 7.82±0.084 | 2.70±0.131 | 4.91±0.089 | 9.31 | 15.43 |

**Table 4.5** In-situ monitoring thickness and TEM total thickness

| Item | DLC/a-Si (nm) | SE Total Thickness | TEM Total Thickness |
|---|---|---|---|
| 1 | 2/2 | 3.74 | 3.82 |
| 2 | 2/6 | 8.66 | 8.41 |
| 3 | 4/4 | 8.63 | 8.47 |
| 4 | 6/2 | 8.29 | 8.23 |
| 5 | 9/6 | 15.43 | 15.66 |

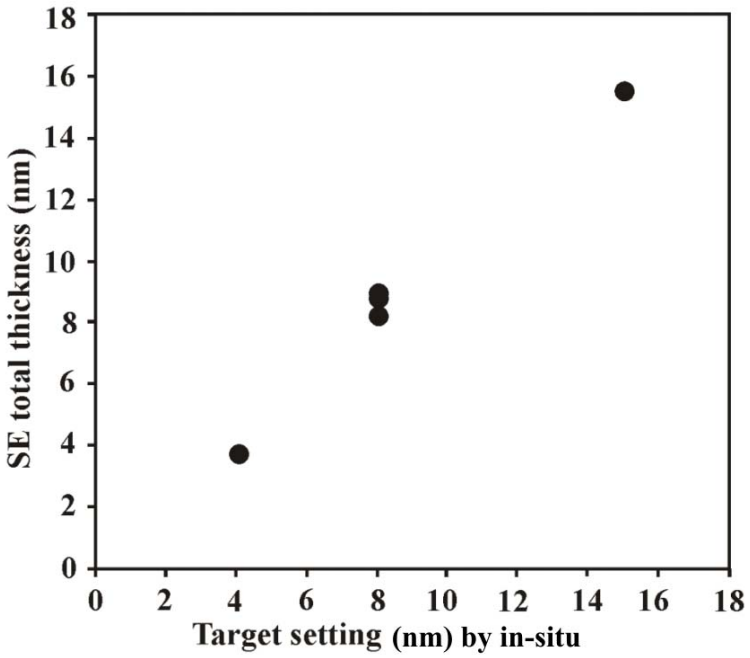


**Figure 4.12** Comparison of the thickness as monitored by *in-situ* ellipsometer and SE total thickness.

The total thicknesses using ex-situ ellipsometer are good agree with TEM. BEMA can estimate interface layer between Si and C only for thick a-Si seed layer. It cannot estimate interface layer for thin a-Si. This phenomena is still unknown and needed for future study.

### 4.1.3 Further DLC Bonding Study with Raman Spectroscopy

The Raman spectra between 1130 and 1800 $cm^{-1}$ of bi-layer film stack of DLC/a-Si on Ge coupon. Two peak centers around 1550 $cm^{-1}$ and 1350 cm-1 were of interest since they corresponded to ordered $sp^2$ carbon arrangements such as in graphite (G) and disordered $sp^2$ carbon (D), respectively. The G peak is due to the bond stretching of all pairs of $sp^2$ atoms in both ring and chains. The D peak is due to the breathing mode of $sp^2$ atoms in ring [89, 93-96]. Collected Raman spectra were analyzed and quantified by fitting with Gaussian profiles in order to categorize them according to G and D peak attributions.

Per the model as developed by Ferrari and Robertson [89], here are some of the key G and D peak features that can be used to elucidate the nature of DLC chemistry using visible Raman spectroscopy. A smaller value of intensity D to intensity G ($I_D/I_G$) which high G peak position corresponds to higher $sp^3$ content. The DLC films thickness can be quantify using the intensity of G peak ($I_{G)}$ [97]. Based on this formulation, we tabulated the analysis result from our film stacks in Table 4.6

**Table 4.6** Raman information extracted from Raman spectra

| DLC/a-Si thickness ratio | Total thickness (nm) | G Wavenumber($cm^{-1}$) | $I_G$ | $I_D/I_G$ | $A_D+A_G$ |
|---|---|---|---|---|---|
| 2/2 | 4 | 1552 | 40.44 | 1.528 | 16897 |
| 2/6 | 8 | 1552 | 47.63 | 1.507 | 23250 |
| 4/4 | 8 | 1557 | 117.77 | 0.744 | 47249 |
| 6/2 | 8 | 1561 | 162.39 | 0.568 | 69818 |
| 9/6 | 15 | 1565 | 385.38 | 0.453 | 154267 |

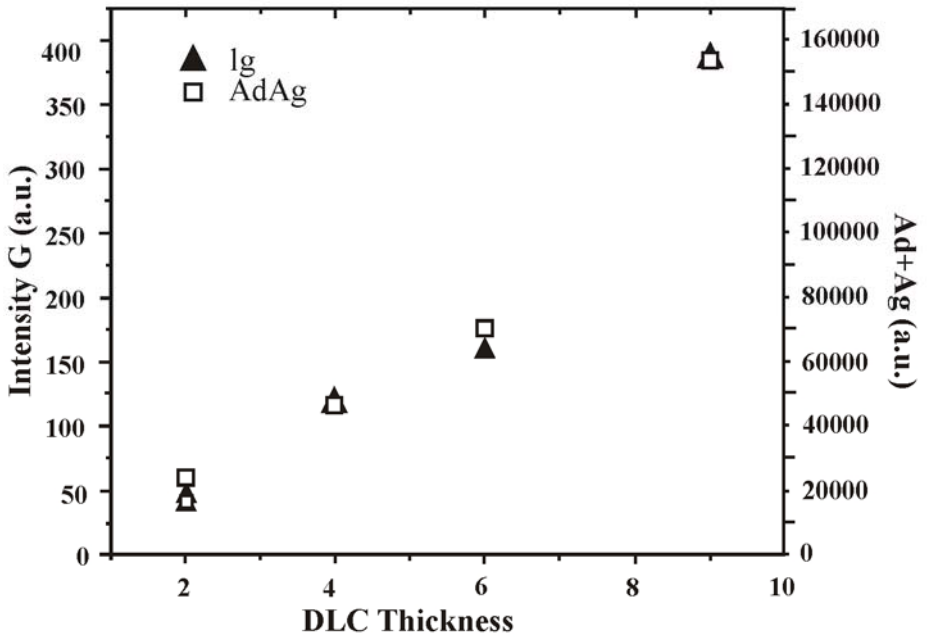


**Figure 4.13** Variation of intensity G and $A_D+A_G$ with DLC thickness of film stack.

Plots of $I_D$ and $I_G$ as a function of DLC thickness. From the plot we can see that the relationship between the DLC thicknesses as controlled by in-situ ellipsometer and intensity G is linear as shown in Figure 4.13. Thus, using an empirical model, the DLC thickness of unknown sample in this thickness range can be computed. It is expect that the intensity G increase with film thickness and eventually saturate when film thickness become grater than the focusing depth of Raman laser beam. Moreover, it was observed that the area under curve D and G ($A_D+A_G$) also correlated with DLC films thickness which is less sensitive to signal to noise ratio of DLC spectra. The $I_D/I_G$ is seen to decrease from 1.13 to 0.45, however G-peak position was upper shift from 1530 $cm^{-1}$ to 1560 $cm^{-1}$ when the DLC film thickness increased from 2 to 9 nm (as controlled by in-situ ellipsometer) as shown in Figure 4.14(a) and (b). It shows that the variation of G position and $I_D/I_G$ with the thickness can be divided into two stages. The 4 nm is critical thickness. When the thickness is 2 nm, the G position and $I_D/I_G$ was nearly not changed. But when the thickness is 4 nm, the G position and $I_D/I_G$ shows abrupt change, and then $I_D/I_G$ was stable while G position slightly increase with further increase of DLC thicknesses. Because the G position and $I_D/I_G$ are related to the structure of DLC films, it indicates that the growth mode of bi-layer film stack of DLC/a-Si during the

deposition mainly involves two stages, and the content of $sp^3$ bond in the film becomes higher with increasing thickness [89, 98-101].

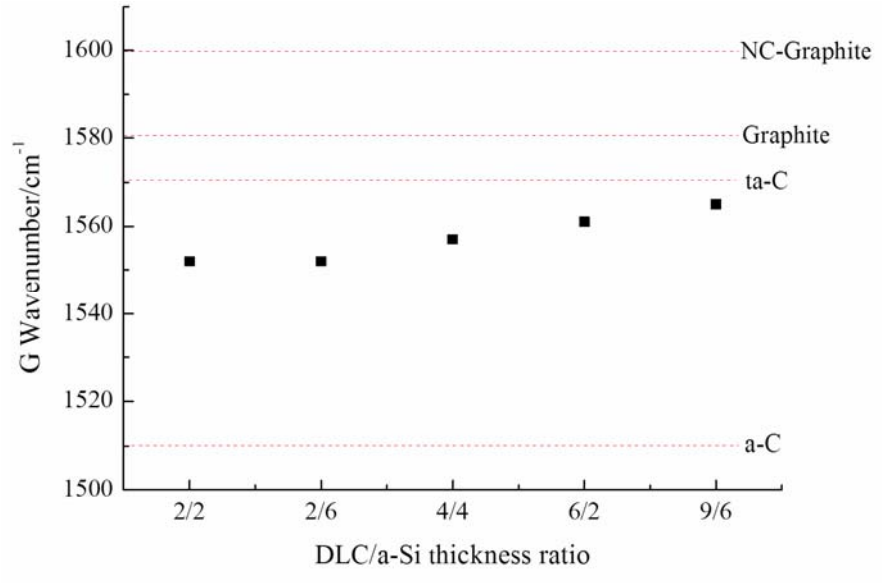


(a)

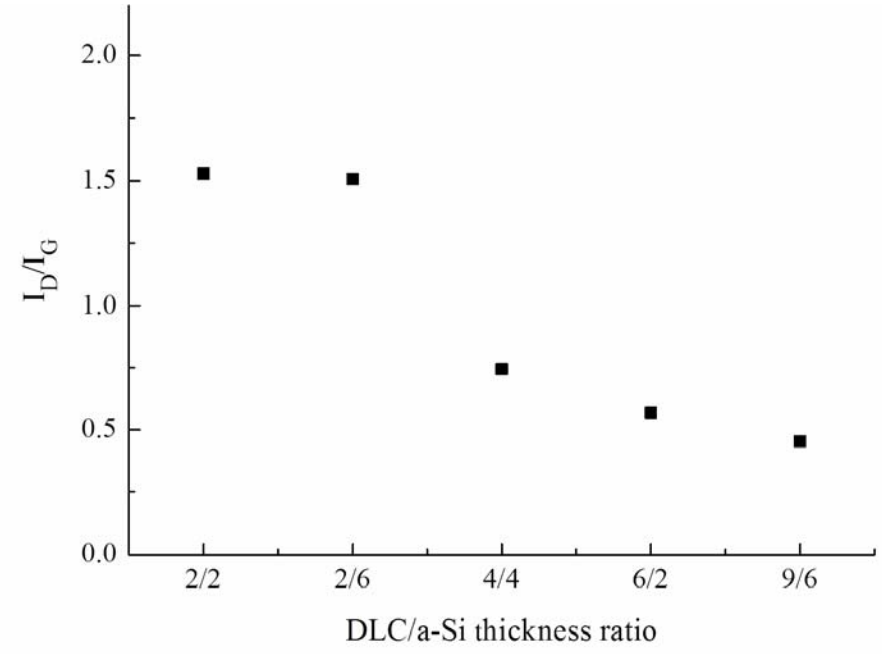


(b)

**Figure 4.14** Variation of G position (a) and $I_D/I_G$ (b) with DLC thickness of film stack.

## 4.2 The Results from Various Wafer Substrate on Germanium, Tantalum and Silicon

Surface energy of the substrate was analyzed with regard to contact angle measurement. It is well-known that wetting ability of liquid on a solid surface is controlled by atomic mechanisms occurring at the solid/liquid/vapor interface, depending upon the surface phenomenon between adsorbent and adsorbate, such as adsorption, desorption, diffusion and evaporation [102-103]. Contact angle ($\rho$) can be used as a simple indicator for wetting ability of liquid on a solid surface, i.e. $\rho < 90^o$ and $\rho > 90^o$ determine wetting and non-wetting conditions, respectively. Therefore, prior to the deposition of a-Si and DLC films, contact angles of water droplets on bare $SiO_2$, Ge and $Ta_2O_5$ substrates were measured.

For contact angle measurements, 1-μL water droplet was dropped at 5 different positions on the substrate surface at room temperature and 5 values of contact angle were obtained. The average values of contact angle of water droplet on $SiO_2$, Ge and $Ta_2O_5$ substrates are given in Table 4.7. The typical photographs of 1- μL water droplet on $SiO_2$, Ge and $Ta_2O_5$ substrates are shown in Figure 4.15(a)-(c). As shown in Table 4.7 and Figure 4.15(a)-(c), contact angles of 1-μL water droplets on $SiO_2$, Ge and $Ta_2O_5$ substrates are approximately 53°, 63° and 75°, respectively. The angle also gives information on the surface energy of the substrate. The lower the contact angle corresponds to the higher the surface energy of the solid material. Thus, $SiO_2$ substrate has the highest surface energy (Figure 4.15(d)), whereas $Ta_2O_5$ substrate has the lowest surface energy (Figure 4.15(e)).

**Table 4.7** Contact angles of water droplet (1μL) and root mean square (RMS) roughness of the bare substrates. The average contact angle from each substrate was measured from 5 different positions on the substrate surface at room temperature

| Substrate | Contact angle (degree) | RMS roughness, scanning area of 1μm x1 μm (nm) |
|---|---|---|
| $SiO_2$ | 52.92 ± 0.89 | 0.31 |
| Ge | 63.02 ± 1.52 | 2.83 |
| $Ta_2O_5$ | 75.30 ± 1.23 | 0.33 |

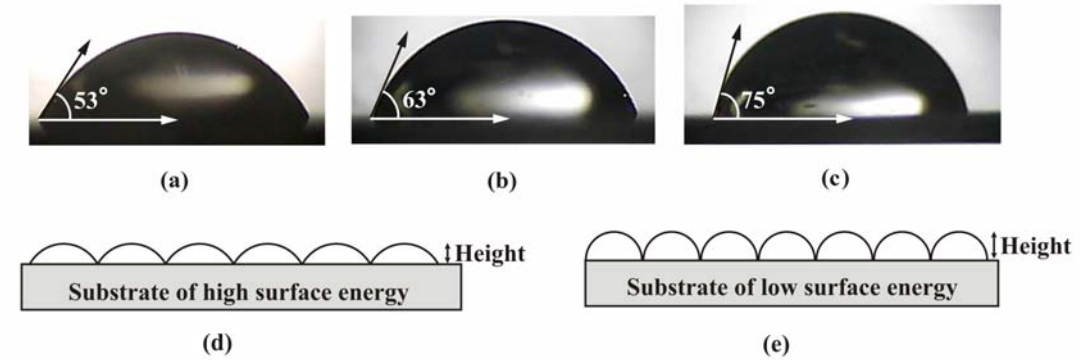


**Figure 4.15** Contact angle of water droplet (1μL) on different substrates: (a) $SiO_2$ (53$^o$), (b) Ge (63$^o$) and (c) $Ta_2O_5$ (75$^o$) Schematics in (d) and (e) show that a-Si may form a droplet-like cluster on the substrate of different surface energies. Surface energy affects the shape and height of droplets.

Figure 4.16 shows the surface morphology of bare $SiO_2$, Ge and $Ta_2O_5$ substrates as investigated by AFM in tapping mode and a scanning area of 1 μm × 1 μm. The root mean square (RMS) roughness of the three substrate surfaces obtained from Figure 4.16 is given in Table 4.7. The RMS roughness of $SiO_2$, Ge and $Ta_2O_5$ was found to be 0.31, 2.83 and 0.33 nm, respectively. The results, however, are not correlated with the contact angle values.

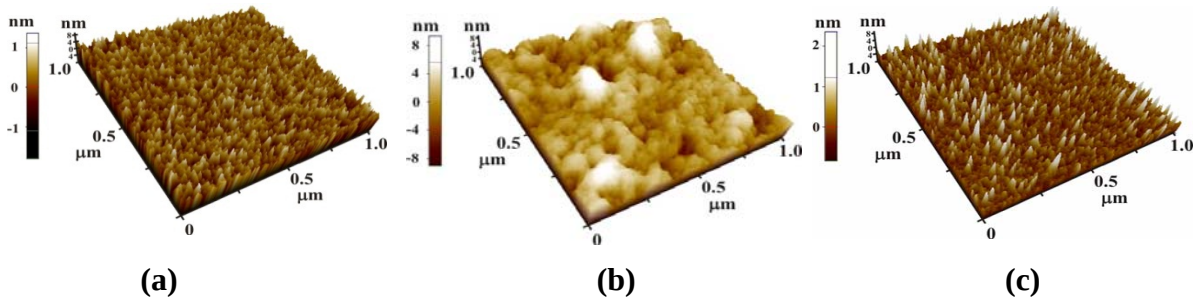


**Figure 4.16** Surface morphology of bare substrates: (a) $SiO_2$, (b) Ge and (c) $Ta_2O_5$.

The growth of DLC/a-Si films on $SiO_2$, Ge and $Ta_2O_5$ substrates was further investigated using TEM. Figure 4.17 shows cross-section bright-field TEM images of DLC/a-Si bilayer film deposited on $SiO_2$, Ge and $Ta_2O_5$ substrates, respectively. The thickness of a-Si and DLC films was determined from Figure 4.17 and the obtained thicknesses are given in Table 4.8. The thicknesses of a-Si layers on $SiO_2$, Ge and $Ta_2O_5$ are 5.64, 6.30 and 6.97 nm, respectively, whereas those of DLC layers on the a-Si layers are the same. To have further understanding on these phenomena, the effect of the adsorbent surface energy on the film-growth mechanism of a-Si layer and DLC film is discussed.

**Table 4.8** Average thickness of a-Si layer, DLC film and root mean square (RMS) roughness of DLC film on different substrates. The thickness of a-Si and DLC films were averaged from 10 positions in TEM image

| Substrate | Average film thickness (nm) | | RMS roughness, scanning area of 1μm x1 μm (nm) |
|---|---|---|---|
| | a-Si | DLC | |
| $SiO_2$ | 5.64 ± 0.14 | 9.91 ± 0.15 | 0.17 |
| Ge | 6.30 ± 0.16 | 9.96 ± 0.19 | 0.30 |
| $Ta_2O_5$ | 6.97 ± 0.17 | 10.02 ± 0.30 | 0.31 |

For the a-Si layer, the difference in thickness may be resulted from the wetting ability of a-Si liquid on the substrate which is a function of the surface energy of the solid/liquid/gas interface. We propose that the early stage of the a-Si film-growing is an important step that affects the overall thickness of the a-Si layer. If we assume that the deposition rates of Si molecules on the three substrates are equal, the growth of a-Si layers on the substrates should be the same unless the substrates have difference magnitude of wetting. At the early stage of the a-Si film-growing, Si atoms or molecules approach and accommodate on the surface of the substrate. Migration and aggregation of Si molecules along the substrate surface begin to form 2D clusters (nanocluster) resembling liquid droplets (or island) on the substrate. Here, the surface energy of the solid substrate plays an important role on the height of the clusters, see Figure 4.15(d) and (e). The clusters continue to grow as a random network until they coalesce and the substrate surface is finally covered with a-Si layer, calling an initial layer. Then, more Si molecules are deposited on this initial layer until the a-Si layer becomes thicker.

The difference in the average thickness of a-Si layer on the substrates may be related to the difference in surface energy of the substrate as previously mentioned. As shown in Figure 4.15, contact angle measurement was employed as a simple methodology to obtain information on surface energy of the substrate. Lower contact angle indicates that the substrate has higher surface energy. Contact angles of water droplet on $SiO_2$, Ge, and $Ta_2O_5$ substrates are approximately 53°, 63° and, 75°, respectively, as shown in Table 4.7 It is seen in Table 4.8 that the thickness of a-Si layer is inversely proportional to the surface energy of the substrate. The thinnest a-Si layer, 5.64 nm, was obtained from $SiO_2$ substrate which has the highest surface energy. The thickest a-Si layer, 6.97 nm, was obtained from $Ta_2O_5$ substrate corresponding to the lowest surface energy. Ge substrate, having the surface energy in the range between those of $SiO_2$ and $Ta_2O_5$ substrates, offered the a-Si layer of 6.30 nm.

The lowest surface energy of $Ta_2O_5$ substrate leads to the thickest a-Si layer because it can build up more globular droplet as shown in Figure 4.15(c) and (e). It is this globular droplet that affects the thickness of the a-Si layer. In contrast, the highest surface energy of $SiO_2$ substrate induced almost flat droplet, see Figure 4.15(a) and (d) and, then, the flat droplet led to the thinnest a-Si layer of 5.64 nm, as shown by cross-section bright-field TEM images in Figure 4.17.

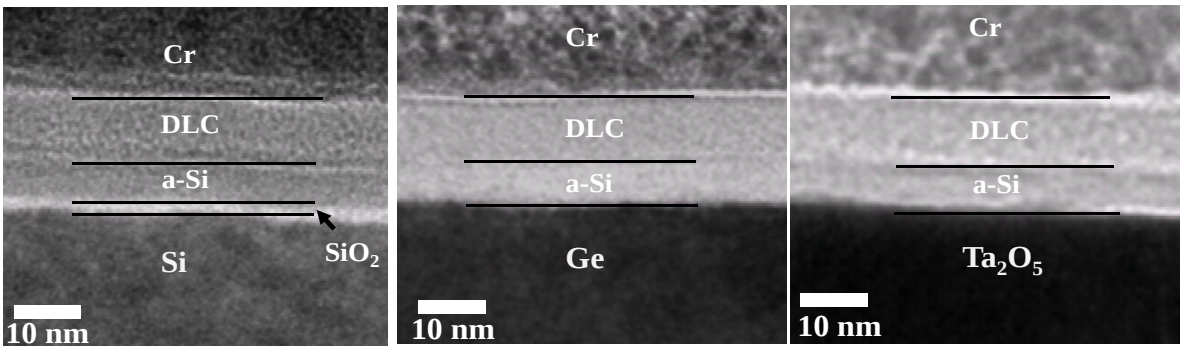


**Figure 4.17** Cross-section bright-field TEM images of a-Si and DLC films deposited on different substrates: (a) $SiO_2$, (b) Ge and (c) $Ta_2O_5$. Note that the thickness of $SiO_2$ layer is only 2 nm due to the growth of native oxide on Si substrate.

DLC film thickness on the three substrates, however, was approximately the same with 9.9 nm thick, as shown in Table 4.8 and Figure 4.17. This is due to the DLC films grown on the a-Si layers of three substrates with equivalent surface energy of a-Si layers. As previous discussion on the early stage of the growth of a-Si layer, the growth of DLC film is also similar to that of a-Si layer. The wetting ability of DLC molecules on the a-Si layer from each substrate was the same. Thus, the thicknesses of the DLC films from different substrates are similar. Figure 4.18 shows three-dimensional images of DLC films on different substrates obtained from atomic force microscopy (AFM, 1μm x 1μm). The values of the RMS roughness of the DLC films on $SiO_2$, Ge and $Ta_2O_5$ substrates are 0.17, 0.30, and 0.31 nm, respectively. The little difference in the RMS roughness of the DLC films may be due to the difference in the initial roughness values of the bare substrates.

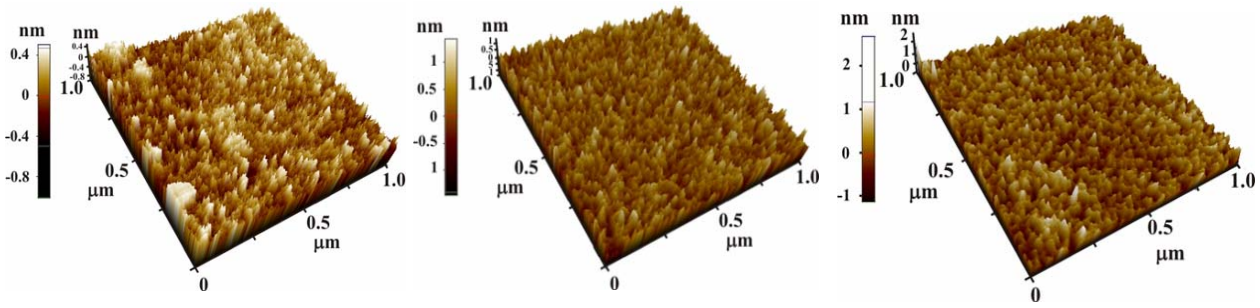


**(a)** **(b)** **(c)**

**Figure 4.18** Surface topography of DLC film on different substrates: (a) $SiO_2$, (b) Ge, and (c) $Ta_2O_5$. The data were obtained from AFM measurements.